



## Original Article

# Investigations on TiO<sub>2</sub>-NiO@In<sub>2</sub>O<sub>3</sub> Nanocomposite Thin Films (NCTFs) for Gas Sensing: Synthesis, Physical Characterization, and Detection of NO<sub>2</sub> and H<sub>2</sub>S Gas Sensors

M. Abd Shahoodh<sup>1</sup>, F.T. Ibrahim<sup>2,\*</sup> , S. Guermazi<sup>3</sup>

<sup>1</sup> Ministry of Education, Anbar Education Directorate, Anbar, Iraq

<sup>2</sup> Physics Department, College of Science, University of Baghdad, Baghdad, Iraq

<sup>3</sup> Laboratory of Materials for Energy and Environment, and Modeling (LMEEM), Faculty of Sciences of Sfax, University of Sfax, B.P: 1171, 3038, Tunisia

## ARTICLE INFO

## Article history

Submitted: 2023-10-03

Revised: 2023-11-04

Accepted: 2023-12-11

Manuscript ID: CHEMM-2312-1741

Checked for Plagiarism: Yes

Language Editor:

Dr. Fatimah Ramezani

Editor who approved publication:

Dr. Lotf Ali Saghatforoush

DOI:10.48309/chemm.2023.428217.1741

## KEYWORDS

TiO<sub>2</sub>-NiO@In<sub>2</sub>O<sub>3</sub> NCTFs /glass substrate

Crystal structure

High sensitivity

NO<sub>2</sub> and H<sub>2</sub>S gas sensors

Optical properties

## ABSTRACT

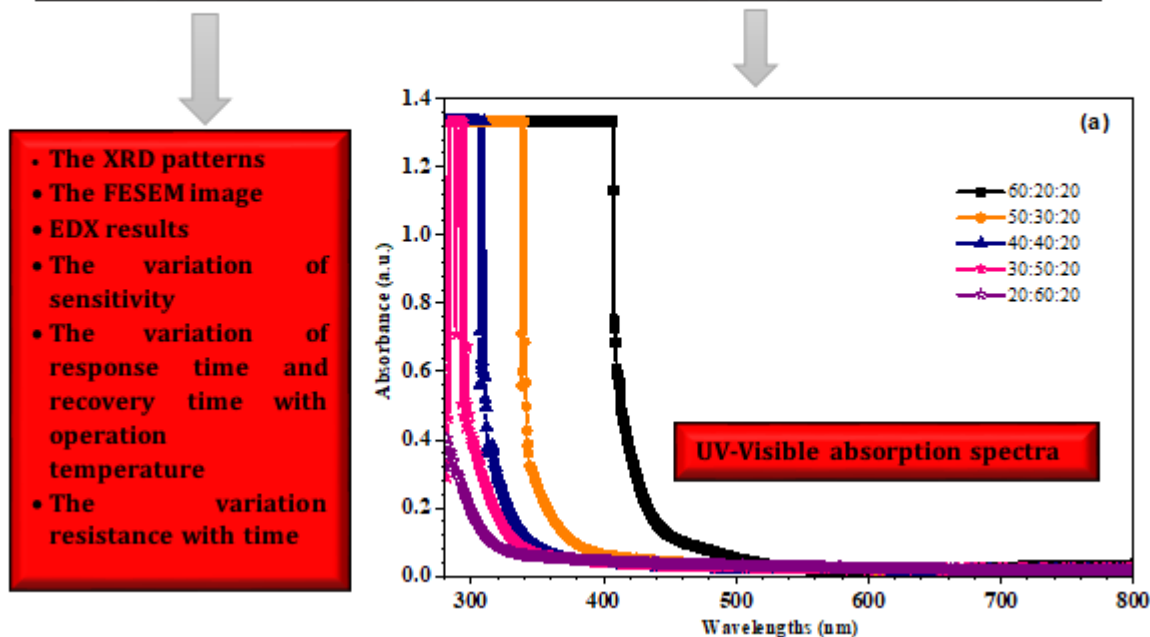
The spray pyrolysis technique is a versatile and cost-effective method for producing TiO<sub>2</sub>-NiO@In<sub>2</sub>O<sub>3</sub> NCTFs on glass substrates with varying molar ratios. NCTFs have been studied for gas-sensing applications due to their excellent sensing properties. The films' structural, morphological, and gas-sensing characteristics were analyzed. The XRD analysis indicates that the NCTFs are polycrystalline, meaning that they are made up of many small crystals. The crystals are oriented in a random fashion, which is why the XRD pattern is broad. The anatase phase of TiO<sub>2</sub> is a tetragonal crystal structure. The NiO and In<sub>2</sub>O<sub>3</sub> phases are both cubic crystal structures. The presence of nanostructure cubic phases indicates that the nanoparticles in the films are small enough to significantly affect the crystal structure of the films. Scanning electron microscopy images showed surface homogeneity, with small granular grains of nanostructures without any cracks. The gas sensor created using the prepared samples showed high sensitivity to NO<sub>2</sub> and H<sub>2</sub>S gases, and its sensitivity was measured at different operation temperatures, along with response and recovery times. The optical properties of In<sub>2</sub>O<sub>3</sub> are affected by the addition of TiO<sub>2</sub> and NiO impurities. The In<sub>2</sub>O<sub>3</sub> transmittance increases as the NiO ratio increases and the TiO<sub>2</sub> ratio decreases.

\* Corresponding author: F.T. Ibrahim

✉ E-mail: [fuadtariq1975@gmail.com](mailto:fuadtariq1975@gmail.com)

© 2023 by SPC (Sami Publishing Company)

## TiO<sub>2</sub>-NiO@In<sub>2</sub>O<sub>3</sub> Nanocomposite Thin Films (NCTFs)



### Introduction

Thin-film semiconductor gas sensors are becoming increasingly popular for various applications, including environmental monitoring, industrial safety, and medical diagnostics. They offer a few advantages over other types of gas sensors, including high sensitivity, fast response time, and low cost. The high sensitivity and trustworthiness of thin-film semiconductor gas sensors make them ideal for applications where it is important to detect even very low concentrations of gases. They can be used to detect hazardous gases in the workplace, monitor air quality, and diagnose medical conditions [1,2]. Metal oxide gas sensors are a cost-effective and suitable option for detecting harmful gases. Various metal oxide gas sensors, ranging from thick to thin films, have been fabricated using metal oxides such as ZnO [3], TiO<sub>2</sub> [4], multilayer-coated (SnO<sub>2</sub>-CuO), and TiO<sub>2</sub>-ZnO composite [5] for sensing H<sub>2</sub>S gas [6]. Recently, low-concentration gas sensors have also been reported [7]. Nanocrystalline metal oxides have attracted a lot of interest in sensing H<sub>2</sub>S gas at room temperature due to their following advantages high surface area, reduced

grain boundaries, and enhanced charge carrier mobility [7]. In addition to these advantages, nanocrystalline metal oxides are also relatively inexpensive to produce, which makes them a cost-effective option for gas-sensing applications. NiO, TiO<sub>2</sub>, and In<sub>2</sub>O<sub>3</sub> are often used for detecting toxic and pollutant gases due to their non-hygroscopic meaning that they do not absorb water from the air. This is an important property for gas sensors, as water vapor can interfere with the sensing process, non-toxic which makes them safe to use in applications, where people are exposed to the sensors, inorganic meaning that they are not made up of organic compounds [8]. This is an important property for gas sensors, as organic compounds can be flammable or explosive, polar meaning that they have a positive and negative end. This polarity allows them to interact with gases and to change their conductivity in the presence of gases, and their crystalline nature means that they have a regular atomic structure. This crystalline structure gives the materials their desired properties, such as high surface area and conductivity [8]. These materials are cheap, safe, and readily available, which makes them beneficial and applied in many devices such as sensors, transparent conductors, and surface acoustic wave devices

[9-11]. These materials are often used in simple devices, such as paper cups and saltshakers. However, they can also be used in more complex devices, such as solar cells and medical implants. Due to their ease of fabrication, affordability, and compactness, these types of sensors are preferred. Metal oxide gas sensors have valence and conduction bands, just like semiconductors [9]. The gas sensing technique relies on the anisotropy of the electrical resistance of metal oxide thin films. The main sensing process involves the change of oxygen concentration on the surface of these metal oxides through adsorption and various catalytic reactions of oxidation and reduction of gaseous species. The electrical conductivity depends on the gas ambience and the sensing material operation temperature when exposed to the test gas [12]. In a conductometric gas sensor, the sensing material is a semiconductor oxide, such as tin dioxide (SnO<sub>2</sub>) or zinc oxide (ZnO). These materials have a high electrical resistance in air, but their resistance decreases when they are exposed to certain gases, such as carbon monoxide (CO), nitrogen dioxide (NO<sub>2</sub>), and hydrogen (H<sub>2</sub>). This is because the gas molecules adsorb onto the surface of the semiconductor oxide and create a depletion layer, which reduces the number of free electrons in the material. This decrease in the number of free electrons leads to a decrease in the electrical conductivity of the material [13]. This study discusses the use of TiO<sub>2</sub>-NiO@In<sub>2</sub>O<sub>3</sub> NCTFs as NO<sub>2</sub> and H<sub>2</sub>S gas sensors at different operation temperatures. Individually, TiO<sub>2</sub>, NiO, and In<sub>2</sub>O<sub>3</sub> films have proven successful in gas sensing applications.

## Experimental

The TiO<sub>2</sub>-NiO@In<sub>2</sub>O<sub>3</sub> NCTFs were prepared on glass substrates heated to 400 °C using the chemical spray pyrolysis technique. Prior to the deposition, there was a predetermined 30 cm gap between the sprayer head and the substrate. The glass substrates (2×2 cm<sup>2</sup>) were cleaned with acetone, ethanol, and deionized water using ultrasonic cleaning for 15 minutes, and then dried in an air oven at 100 °C for one hour. Indium chloride (InCl<sub>3</sub>, purity 99.99%, molecular

weight 221.18 g/mole) and nickel chloride (NiCl<sub>2</sub>, quality 99.99%, molecular weight 129.5994 g/mole) were dissolved in 100 ml of deionized water to prepare (0.2M). A solution of 100ml with 0.2M titanium trichloride (TiCl<sub>3</sub>, purity of 99.99%, molecular weight of 154.22 g/mole) was also used. The solutions were mixed using a magnetic stirrer until completely dissolved, and the molarity (M) was calculated using Equating (1):

$$M = \frac{Wt}{Mwt} \times \frac{1000}{V} \quad (1)$$

Where, *Wt* is the Weight of salt in grams, *Mwt* is the molar weight typically in grams per mole, and *V* is the volume of the solution typically in liters. The NCTFs with various TiO<sub>2</sub>-NiO@In<sub>2</sub>O<sub>3</sub> molar ratio 20:60:20, 30:50:20, 40:40:20, 50:30:20, and 60:20:20 were prepared. Field Emission Scanning Electron Microscope (FESEM) analysis (Inspect F50 FEI Company) is used to examine the surface morphology and composition of materials at high magnifications. It can be used to study the size, shape, and distribution of particles, as well as the presence of defects and other features on the surface of a material. The structure of the samples was then studied by XRD (6000 SHIMADZ) to determine the crystal structure and average crystallite size. The diffraction scans were collected over a (2θ) range varying from (10° to 80°) with CuK radiation. The sensing performance of the sensors to NO<sub>2</sub> and H<sub>2</sub>S test gas was examined using a homemade gas-sensing system. The sample under test was heated using an electrical hot plate, and the effect of changing operating temperatures on sensing characterization was studied by regulating the variable electrical resistance used to control the electrical current passing through the hot plate element. The operating temperature of the sensor was monitored using a K-type thermocouple. A gas flowmeter was used to achieve the required gas concentration in the test chamber, and a digital millimeter (Victor 86B) was used to measure the change in resistance of the sample under test. After every gas exposure cycle, the air was allowed to pass into the test chamber for a refresh. The Lambda 365 is a double-beam UV-

Vis spectrophotometer that can measure absorbance in the wavelength range of 190-1100 nm. It is a versatile instrument and a powerful tool for studying the optical properties of TiO<sub>2</sub>-NiO@In<sub>2</sub>O<sub>3</sub> NCTFs that can be used for various applications, including the measurement of UV absorption.

It can be used to optimize the optical properties of the TiO<sub>2</sub>-NiO@In<sub>2</sub>O<sub>3</sub> NCTFs for specific applications. The FluoroMax® Plus is a benchtop spectrofluorometer from HORIBA that is designed for the detection of emission spectra out to 1700 nm. It has a signal-to-noise ratio of 10.000:1 and is equipped with a xenon source.

## Results and Discussion

### Morphological properties

The polycrystallinity phase of the samples was confirmed by X-ray diffraction. The XRD patterns of the TiO<sub>2</sub>-NiO@In<sub>2</sub>O<sub>3</sub> NCTFs obtained at different concentrations on glass substrates are

displayed in Figure 1. All the observed diffraction peaks in these XRD patterns are well matched with tetragonal structure TiO<sub>2</sub> anatase according to the standard JCPDS card No. 96-900-9087 ( $a=3.785\text{\AA}$ ,  $c=9.514\text{\AA}$ , space group  $I4_1^1$  md) [14,15], additional diffraction peaks corresponding to the NiO cubic phase according to the JCPDS card No.96-432-0488 ( $a=4.183\text{\AA}$ , space group  $Fm\bar{3}m$ ) [16,17]. In addition to TiO<sub>2</sub> and NiO diffraction peaks, the XRD patterns reveal additional diffraction peaks characteristic of the In<sub>2</sub>O<sub>3</sub> cubic phase in agreement with the JCPDS Card data Card No.96-101-0488 ( $a=10.122\text{\AA}$ , space group  $I_{213}$ ) [18,19].

Table 1 provides X-ray diffraction (XRD) data for different NCTFs with varying ratios of TiO<sub>2</sub>, NiO, and In<sub>2</sub>O<sub>3</sub>. In the context of X-ray diffraction (XRD), the FWHM of a peak can be used to estimate the crystallite size of the material that is being analyzed. The Scherrer equation is a mathematical formula that can be used to

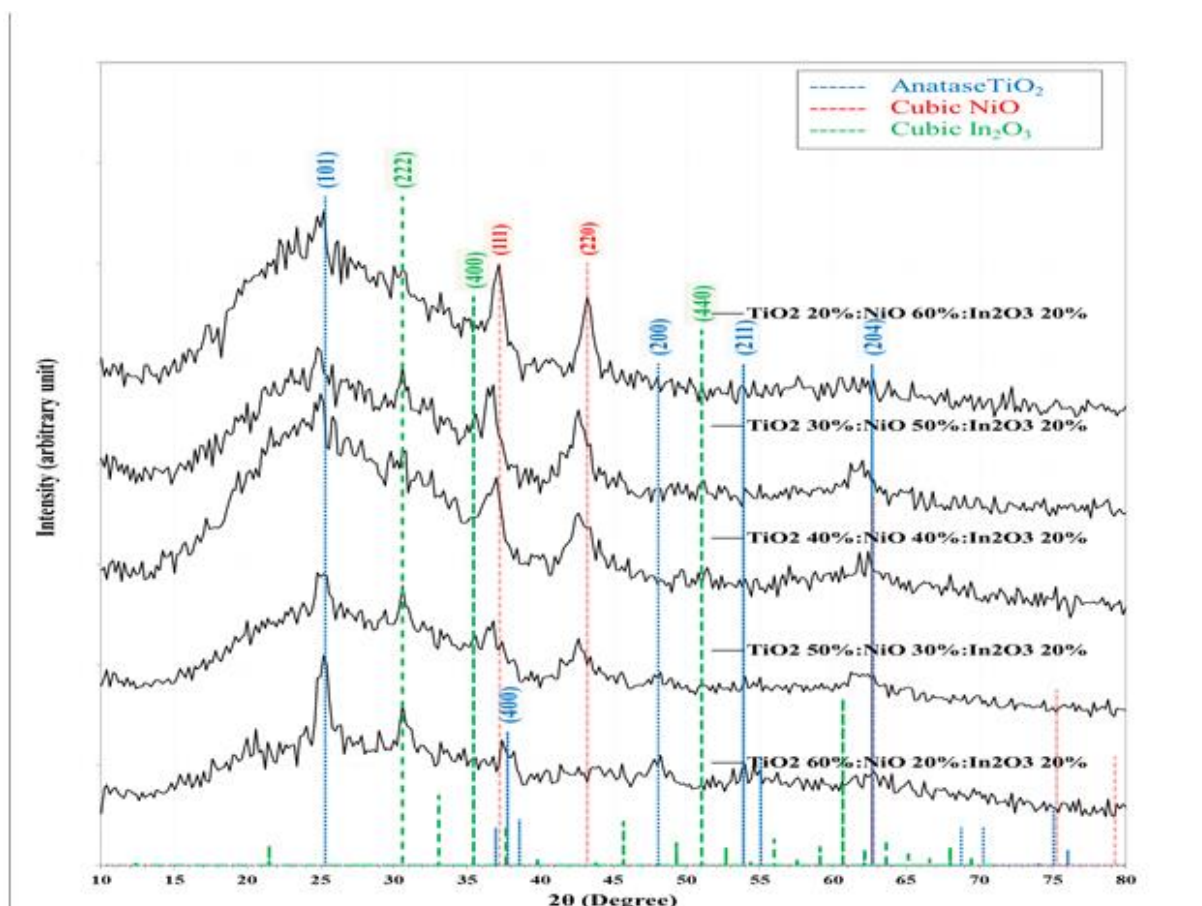


Figure 1: XRD of the TiO<sub>2</sub>-NiO@In<sub>2</sub>O<sub>3</sub> NCTFs on glass substrate

calculate the crystallite size from the FWHM of an XRD peak, as described in Equation (2) [20]:

$$D = \frac{K\lambda}{\beta \cos\theta} \quad (2)$$

Where,  $\lambda = 1.5418 \text{ \AA}$  for Cu radiation,  $\theta$  is the diffraction angle,  $K = 0.9$ , and  $\beta$  is the FWHM. The  $d_{hkl}$  value is related to the spacing between crystal planes, and the (hkl) values correspond to the Miller indices of the crystal planes that are responsible for the diffraction peak. The  $D$  value represents the average size of the crystallites in the sample. Comparing the results of different nanocomposites, we can see that the values of  $2\theta$ , FWHM, and  $d_{hkl}$  vary with the changing ratios of the constituent materials. For example, the peak

at  $25.2348^\circ$  (110) of  $\text{TiO}_2$  is observed in all the nanocomposites, but the  $d_{hkl}$  value changes from  $3.52638 \text{ \AA}$  to  $3.54855 \text{ \AA}$ , as the NiO content increases from 20% to 60%. Similarly, the peak at  $30.6472^\circ$  (222) of  $\text{In}_2\text{O}_3$  is observed in all the nanocomposites, but the FWHM value changes from 0.8820 to 0.9221 as the  $\text{TiO}_2$  content decreases from 60% to 20%. The  $D$  values also vary with the composition of the nanocomposites. The  $D$  value of the (111) peak of NiO decreases from 11.6 nm to 6.8 nm as the  $\text{TiO}_2$  content decreases from 40% to 20%. To sum up, increasing the amount of NiO in the nanocomposite helps in promoting crystallization and reducing the crystallites size,

**Table 1:** Comparison between the Experimental and standards value of  $d_{hkl}$  for the peaks shown in XRD

Samples $\text{TiO}_2\text{-NiO@In}_2\text{O}_3$ NCTFs	$2\theta$ (Deg.)	FWHM (Deg.)	$d_{hkl}$ Exp.( $\text{\AA}$ )	D (nm)	Phase	hkl	Card No.
60:20:20	25.2348	0.9221	3.52638	8.8	Anatase	(110)	96-900-9087
	30.6472	0.8820	2.91482	9.3	Cub. $\text{In}_2\text{O}_3$	(222)	96-101-0589
	37.5430	1.1226	2.39376	7.5	Anatase	(200)	96-900-9087
	47.9668	1.0023	1.89509	8.7	Anatase	(400)	96-900-9087
	53.9404	0.8420	1.69847	10.6	Anatase	(211)	96-900-9087
	62.7205	1.1226	1.48016	8.3	Anatase	(204)	96-900-9087
50:30:20	25.0745	1.0423	3.54855	7.8	Anatase	(110)	96-900-9087
	30.6071	0.8018	2.91855	10.3	Cub. $\text{In}_2\text{O}_3$	(222)	96-101-0589
	36.7010	0.7217	2.44672	11.6	Cub. NiO	(111)	96-432-0488
	42.5544	1.2027	2.12274	7.1	Cub. NiO	(220)	96-432-0488
	48.0069	1.2027	1.8936	7.2	Anatase	(200)	96-900-9087
	53.9805	0.5613	1.6973	15.9	Anatase	(211)	96-900-9087
40:40:20	25.0745	0.8419	3.54855	9.7	Anatase	(110)	96-900-9087
	30.5269	0.8420	2.92603	9.8	Cub. $\text{In}_2\text{O}_3$	(222)	96-101-0589
	36.9015	1.2027	2.43389	7.0	Cub. NiO	(111)	96-432-0488
	42.4742	1.3230	2.12656	6.4	Cub. NiO	(220)	96-432-0488
	51.4147	0.6414	1.77581	13.7	Cub. $\text{In}_2\text{O}_3$	(440)	96-101-0589
	62.4399	0.6816	1.48613	13.6	Anatase	(204)	96-900-9087
30:50:20	24.7938	0.8018	3.58809	10.1	Anatase	(110)	96-900-9087
	30.5670	0.8820	2.92228	9.3	Cub. $\text{In}_2\text{O}_3$	(222)	96-101-0589
	35.6586	0.7217	2.51582	11.6	Cub. $\text{In}_2\text{O}_3$	(400)	96-101-0589
	36.6609	0.9221	2.44931	9.1	Cub. NiO	(111)	96-432-0488
	42.5544	1.0424	2.12274	8.2	Cub. NiO	(220)	96-432-0488
	51.0538	0.8018	1.78751	11.0	Cub. $\text{In}_2\text{O}_3$	(440)	96-101-0589
	61.9989	1.3631	1.49564	6.8	Anatase	(204)	96-900-9087
20:60:20	25.0745	0.8820	3.54855	9.2	Anatase	(110)	96-900-9087
	30.4868	0.9221	2.92979	8.9	Cub. $\text{In}_2\text{O}_3$	(222)	96-101-0589
	37.1821	0.8821	2.41616	9.5	Cub. NiO	(111)	96-432-0488
	43.2360	1.0424	2.09084	8.2	Cub. NiO	(220)	96-432-0488

while the presence of  $\text{In}_2\text{O}_3$  does not seem to have a significant effect.

The FESEM image of  $\text{TiO}_2\text{-NiO@In}_2\text{O}_3$  NCTFs (Figure 2) displays grass-like structures of nanoscale size. These structures exhibit homogeneous distribution with minimal voids and are aligned. In addition, polyhedral shells are present on the surface, distributed depressively on the substrate, with some lining up along the nanoparticle. The FESEM image reveals the

presence of small granular grains on the surface, which are evenly distributed and devoid of any cracks. However, some white-colored patches can be observed on the film surface, possibly due to incomplete decomposition of the precursor salt. Furthermore, spherical grains with a size of 20-100 nm are visible, though FESEM data indicates that the grain size is larger than that estimated from XRD data.

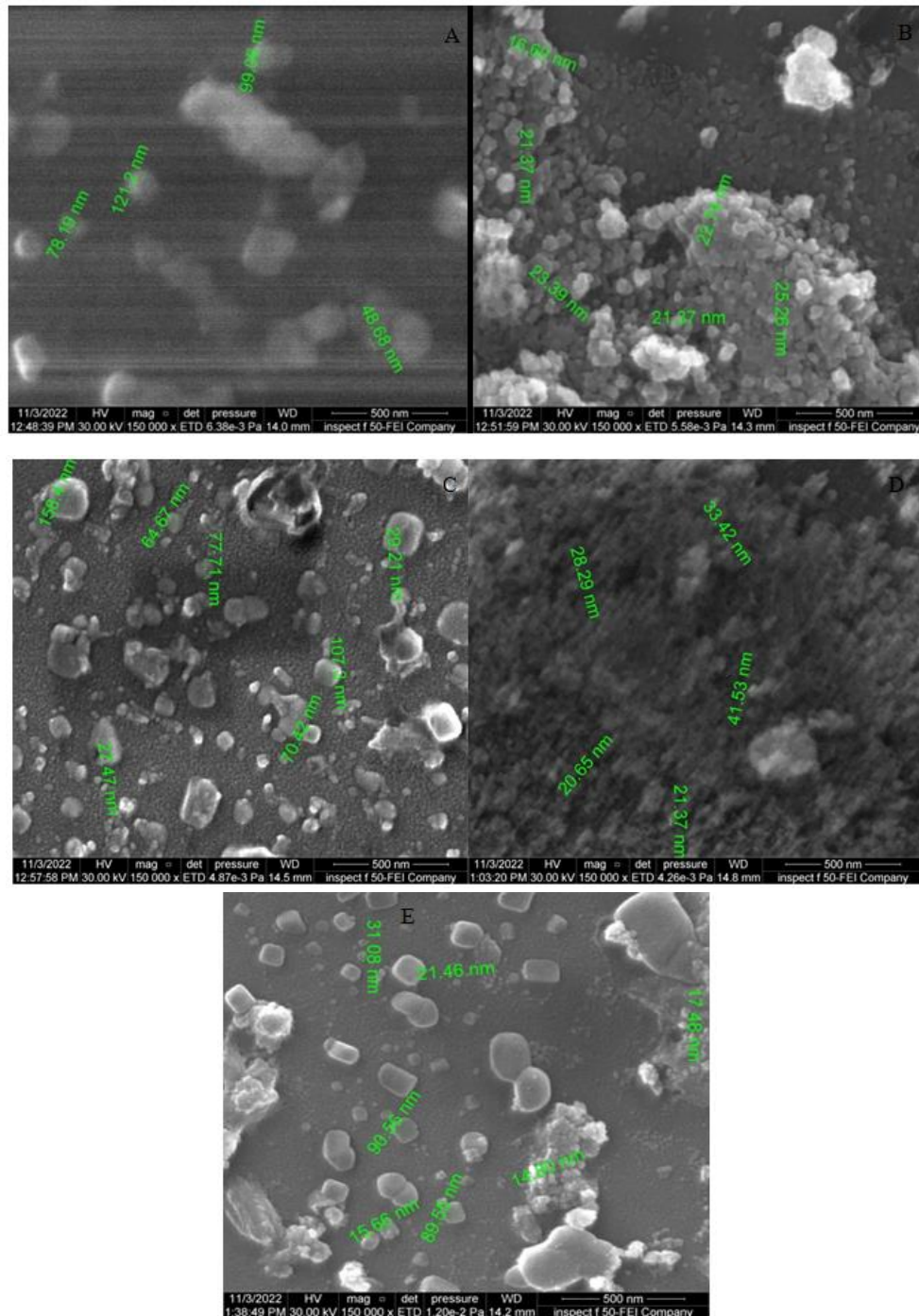


**Figure 2:** FESEM micrographs of  $\text{TiO}_2\text{-NiO@In}_2\text{O}_3$  NCTFs molar ratio: (A) 50:30:20, (B) 40:40:40, (C) 30:50:20, (D) 20:60:20, and (E) 60:20:20, respectively

Energy-dispersive X-ray spectroscopy (EDX) was employed to examine the composition of the samples that were examined by FESEM and XRD. EDX is a technique that can be used to identify the elements present in a material and to determine their relative concentrations. It works by shining a beam of electrons onto a sample and measuring the energy of the X-rays that are emitted. The different energies of the X-rays are characteristic of the different elements that are present in the sample. EDX was employed to analyze the composition of the synthesized  $\text{TiO}_2\text{-NiO@In}_2\text{O}_3$  NCTFs. The resulting EDX pattern in [Figure 3](#) indicated the presence of Ni, Ti, In, and O, confirming that the nanostructure layer primarily consists of  $\text{TiO}_2$ , NiO, and  $\text{In}_2\text{O}_3$ . The atomic percentages of these elements closely matched their theoretical values, supporting the formation of a  $\text{TiO}_2\text{-NiO@In}_2\text{O}_3$  NCTFs hybrid structure [1,22]. In addition, the EDX trace identified the presence of oxygen (O), silicon (Si), and calcium (Ca) elements in the glass substrate. The spectrum also revealed trace amounts of Cl, which originated from precursor  $\text{TiCl}_3$ , NiCl, and  $\text{InCl}_3$  used in the deposition solution to form Cl atoms in the film.

#### *TiO<sub>2</sub>-NiO@In<sub>2</sub>O<sub>3</sub> NCTFs on a glass substrate sensitivity.*

The sensitivity of the  $\text{TiO}_2\text{-NiO@In}_2\text{O}_3$  NCTFs on a glass substrate to  $\text{NO}_2$  and  $\text{H}_2\text{S}$  gas as a function of temperature (operating at 150, 200, 250, and 300 °C) was examined in [Figure 4](#). The films were studied using oxidizing gas ( $\text{NO}_2$ ) and reducing gas ( $\text{H}_2\text{S}$ ) with a concentration of (70 ppm) and (30 ppm), respectively. The results indicate that the films exhibit good sensitivity at all operating temperatures tested. Specifically, for a sample with a composition of 40:40:20, the highest sensitivity to 30 ppm  $\text{H}_2\text{S}$  was observed at temperatures up to 200 °C, with a value of approximately 93%, while the maximum sensitivity of 70ppm  $\text{NO}_2$  gas was 56.4% at 150 °C operation temperature. This high sensitivity is attributed to the nano-sized nature of the films and the large amount of oxygen absorbed on the sample surface. The study investigated the response time and recovery time of gas sensor

samples made from the  $\text{TiO}_2\text{: NiO: In}_2\text{O}_3$  NCTFs, for detecting  $\text{NO}_2$  and  $\text{H}_2\text{S}$  gases, with different compositional ratios (20:60:20, 30:50:20, 40:40:20, 50:30:20, and 60:20:20). The operating temperature was varied to examine its effect on the response and recovery times of the samples. The study found that increasing the operating temperature led to shorter response and recovery times. Among the different compositional ratios tested, the 4:4:2 sample exhibited the fastest response time (4.5s) for  $\text{NO}_2$  gas and (6.3s) for  $\text{H}_2\text{S}$  gas when operated at a temperature of 200 °C and 300 °C, respectively. The results are demonstrated in [Figure 5](#). The primary surface reactions in gas sensing mechanisms are represented by chemisorbed oxygen and oxide gas. These reactions involve the adsorption of oxygen on the film surface in two forms: physisorption and chemisorption. At higher temperatures, chemisorption becomes the dominant process. The transition from physisorption to chemisorption necessitates activation energy, which can be attained by increasing the operating temperature. Increasing the temperature has been found to increase the amount of oxygen adsorbed on the sensor surface [22, 23]. In the temperature range of 150-300 °C, both oxygen molecules and oxygen atoms have a significant impact on the electrophysical and gas-sensing characteristics of the prepared samples. The adsorption of oxygen on the surface of metal oxide results in electron trapping, which reduces the charge carrier density and causes an increase in the resistance of the mixed samples. The oxygen ( $\text{O}^-$ ) species on the surface of sample attract electrons, generating depletion layer that extends to both the particles and the surface barrier. The surface barrier plays a crucial role in the sensor's mechanism as it regulates the transfer of electrons between particles and the test gas, ultimately affecting the sensor material's overall resistance. When the sensor sample reaches its optimal operating temperature and oxygen species ( $\text{O}^-$ surf) adsorb, the coverage of oxygen on the sample surface increases, binding more electrons to the conduction band of the samples and raising the barrier. If the sensor sample is then exposed to  $\text{NO}_2$  test gas, this

phenomenon reduces the conductivity or increases the resistance by increasing the depletion region. This effect can be attributed to the interaction between the  $\text{NO}_2$  gas and the oxygen species, which modifies the surface

barrier and alters the transfer of electrons. The  $\text{H}_2\text{S}$  reducing gas has the opposite behavior when interaction between the  $\text{H}_2\text{S}$  gas and the oxygen species [24].

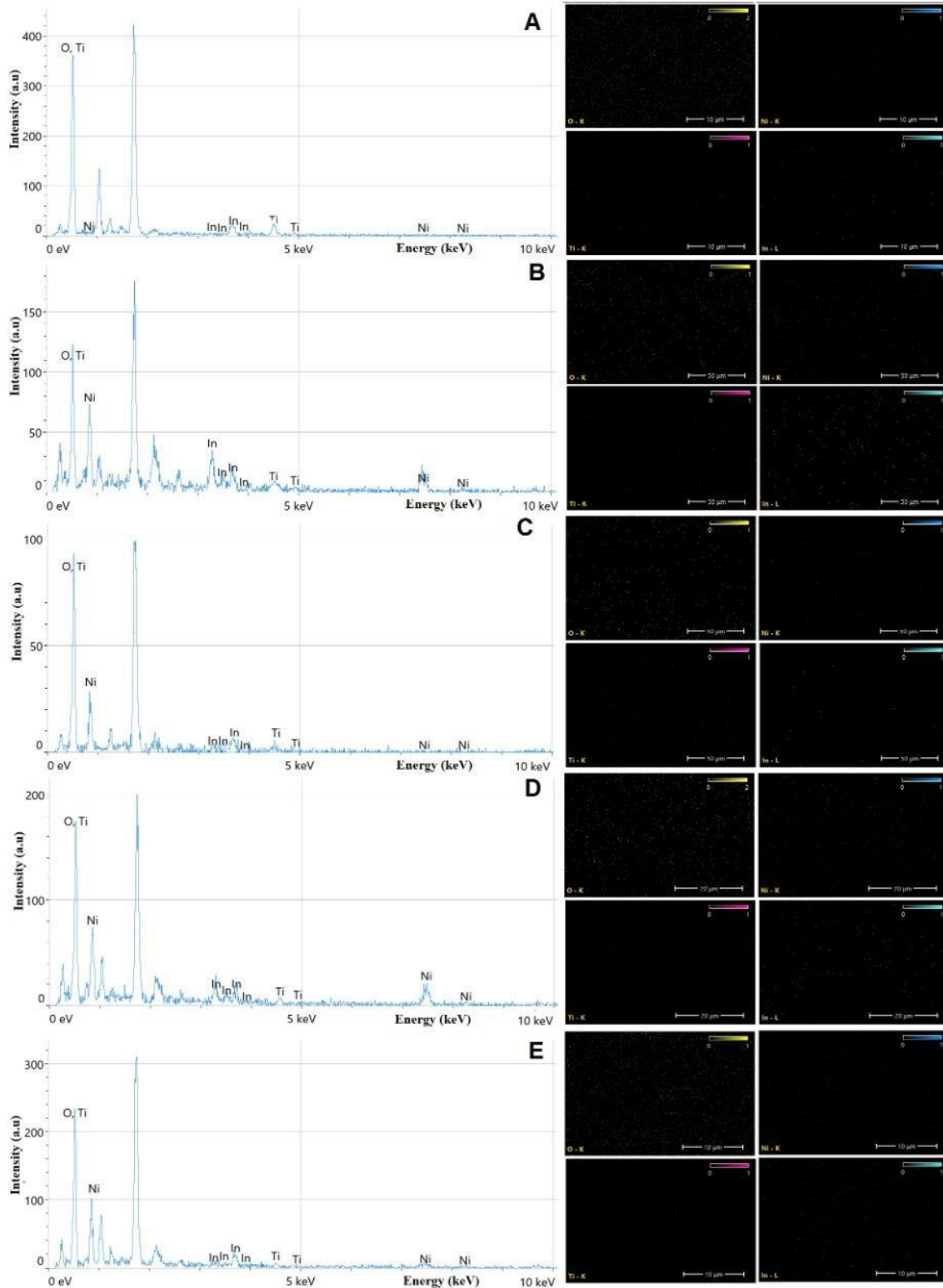


**Figure 3:** EDX results of  $\text{TiO}_2\text{-NiO@In}_2\text{O}_3$  NCTFs molar ratio: (A) 50:30:20, (B) 40:40:40, (C) 30:50:20, (D) 20:60:20, and (E) 60:20:20, respectively

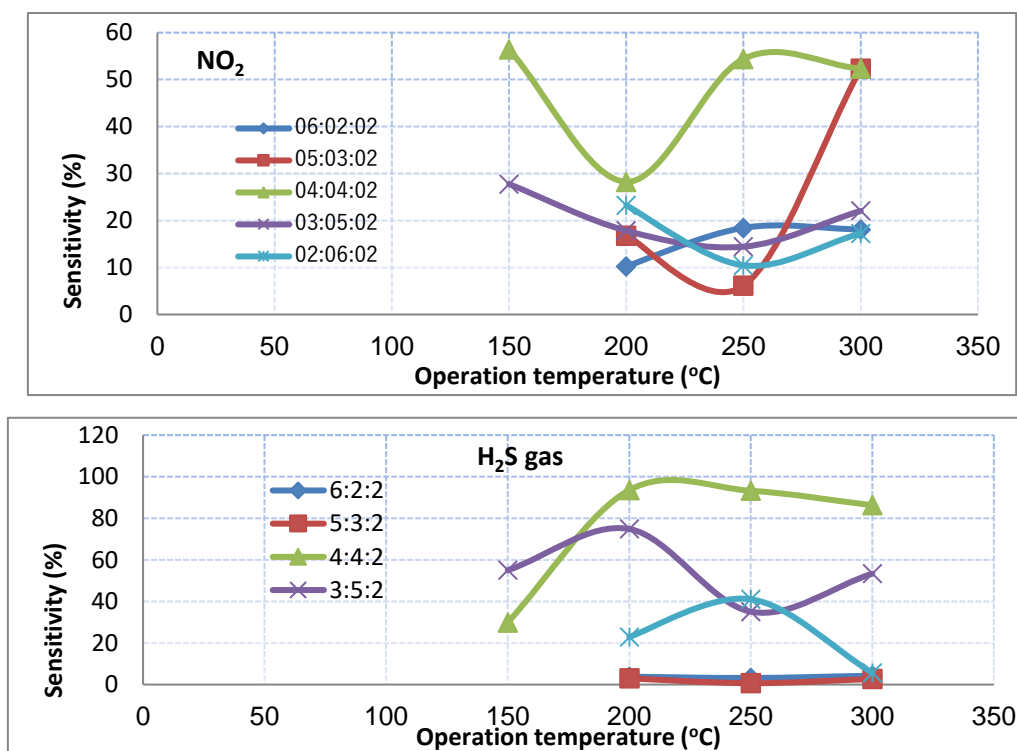


**Figure 4:** The variation of sensitivity with the operating temperature of the prepared, different mixed TiO<sub>2</sub>-NiO@In<sub>2</sub>O<sub>3</sub> NCTFs to NO<sub>2</sub> and H<sub>2</sub>S gases

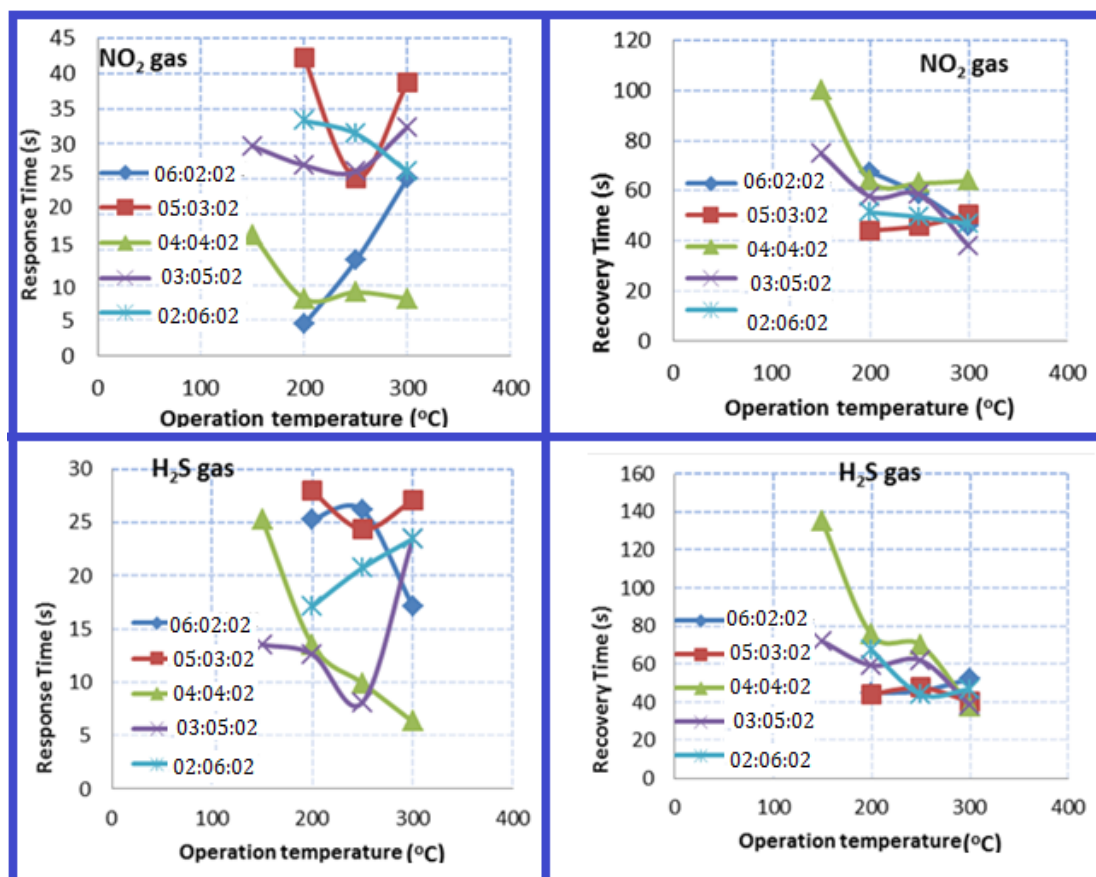


**Figure 5:** The variation of response time and recovery time with operation temperature of the prepared, different mixed TiO<sub>2</sub>-NiO@In<sub>2</sub>O<sub>3</sub> NCTFs to NO<sub>2</sub> and H<sub>2</sub>S gas

Figure 6 describes the response of a TiO<sub>2</sub>-NiO@In<sub>2</sub>O<sub>3</sub> NCTFs (40:40:20) sensor to the presence of NO<sub>2</sub> and H<sub>2</sub>S gases in a testing chamber at ambient air pressure and with a bias voltage of 3V. The sensor's resistance is measured over time, and it is observed that the resistance reaches a steady state before the gas is introduced. Once the H<sub>2</sub>S gas is introduced, the resistance sharply decreases to a new steady state, while introducing the NO<sub>2</sub> gas increases the electrical resistance to a new steady state

indicating that the sensor is detecting the gas presence. When the gases are switched off, the resistance returns to its initial state. The interaction between the surface atoms of the sensing film and the gas molecules is responsible for the sensor's ability to sense the presence of the gas. The NO<sub>2</sub> and H<sub>2</sub>S gas have opposite behavior when interaction with sample surface indicating that the sample has higher selectivity of gases.

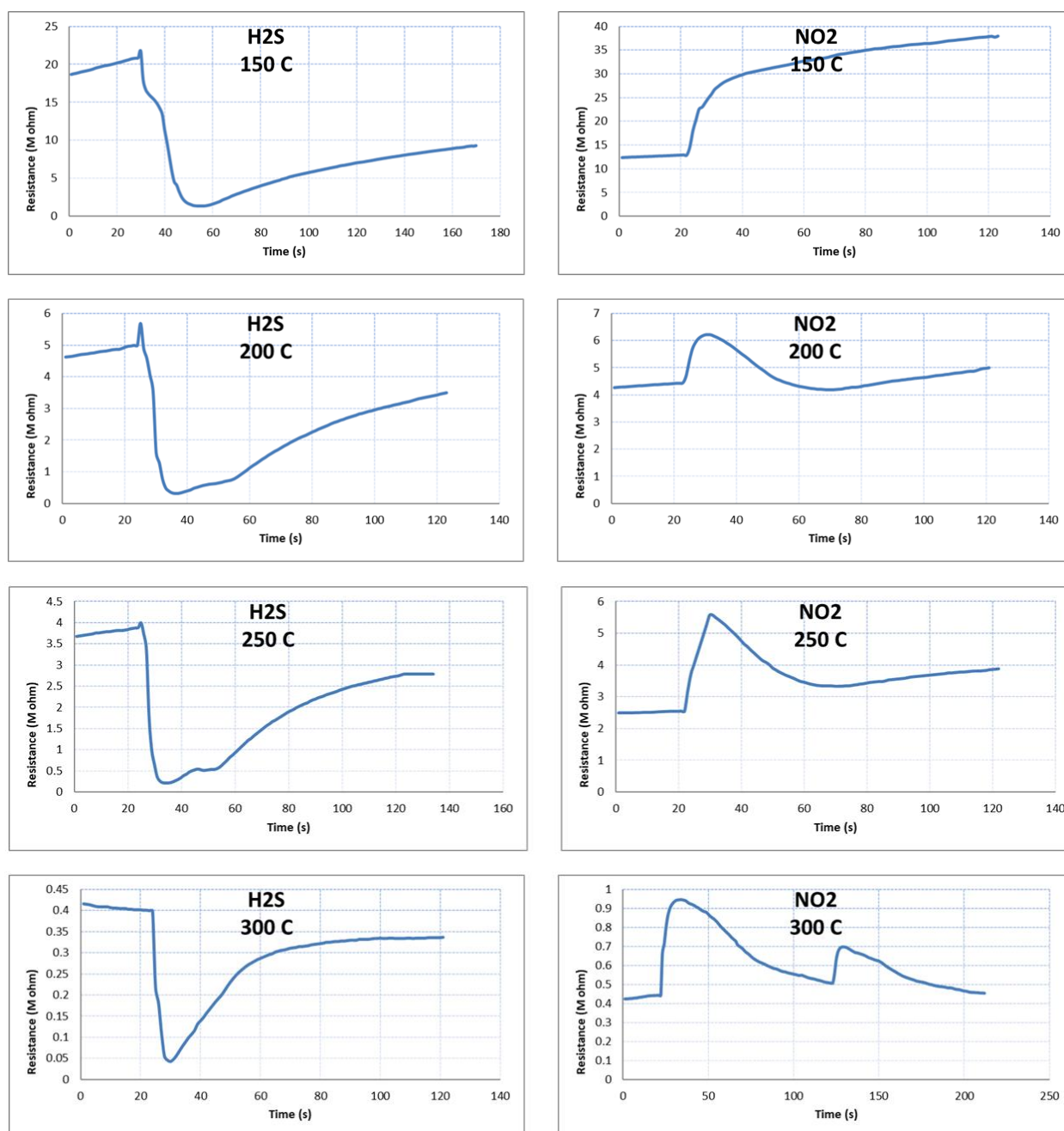
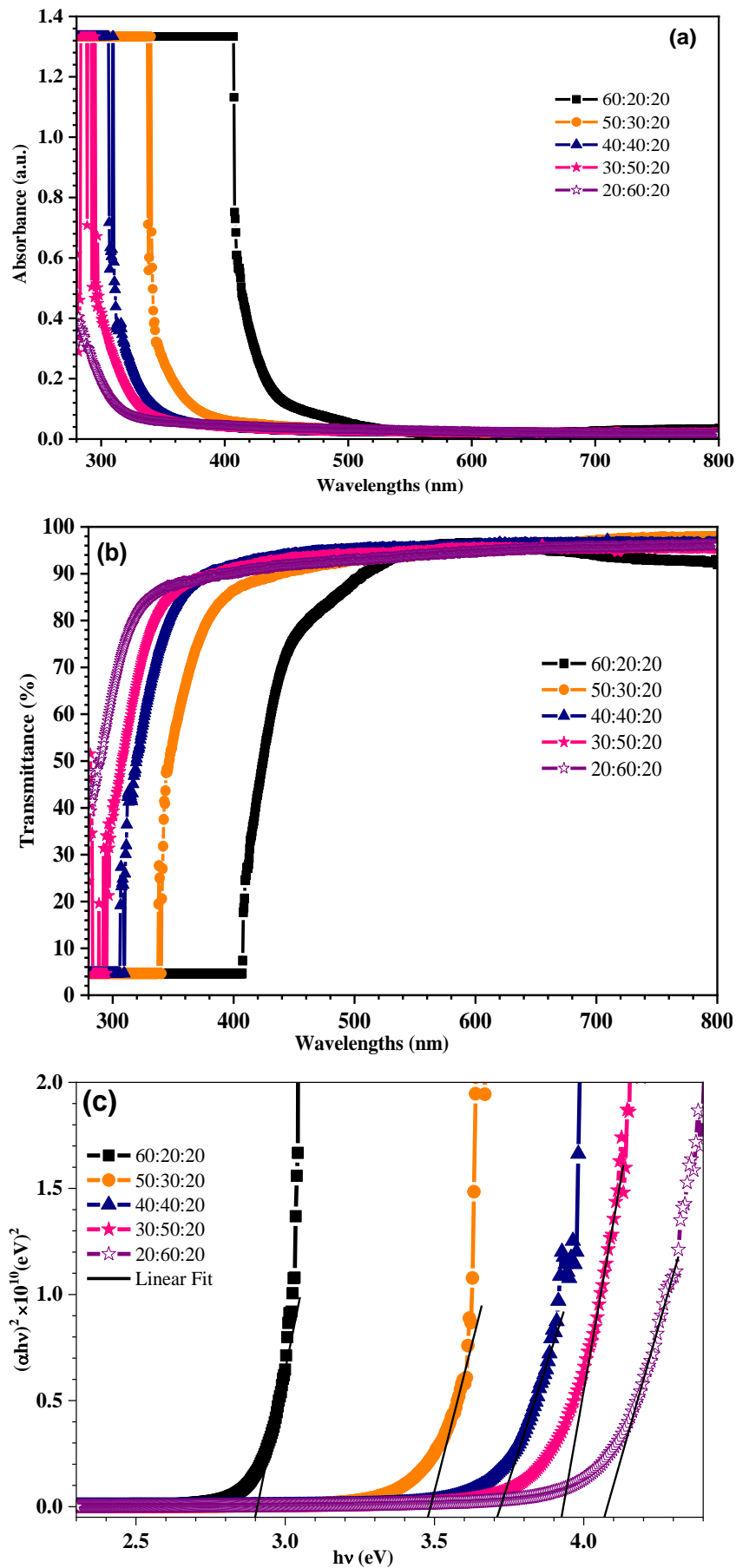


Figure 6: The variation resistance with time for different operation temperature of NO<sub>2</sub> and H<sub>2</sub>S gases for mixed TiO<sub>2</sub>-NiO@In<sub>2</sub>O<sub>3</sub> NCTFs molar ratio: 40:40:20 gas sensor

### Optical study of $\text{TiO}_2\text{-NiO@In}_2\text{O}_3$ NCTFs on a glass substrate

Compared to  $\text{TiO}_2\text{-NiO@In}_2\text{O}_3$  NCTFs (20:60:20), a red shifting in absorption edges towards UV region was observed in the  $\text{TiO}_2\text{-NiO@In}_2\text{O}_3$  NCTFs samples. The results in Figure 7(a) show that the addition of  $\text{TiO}_2$  and NiO to  $\text{In}_2\text{O}_3$  can significantly decrease the absorbance of  $\text{In}_2\text{O}_3$  under visible lights. This is due to the formation of a heterojunction between  $\text{TiO}_2$  and  $\text{In}_2\text{O}_3$ , as well as the presence of NiO, which can donate electrons to  $\text{In}_2\text{O}_3$ . This decrease in absorbance allows  $\text{In}_2\text{O}_3$  to absorb visible light and promote the photocatalytic reactions [25]. This is because  $\text{TiO}_2$  is a wide bandgap semiconductor with an absorption edge in the ultraviolet (UV) region.  $\text{In}_2\text{O}_3$  is also a wide bandgap semiconductor, but its absorption edge is in the visible region. When  $\text{TiO}_2$  and  $\text{In}_2\text{O}_3$  are combined, the two materials form a heterojunction [25]. This heterojunction creates a new bandgap that is smaller than the bandgaps of either  $\text{TiO}_2$  or  $\text{In}_2\text{O}_3$ . This smaller bandgap allows  $\text{In}_2\text{O}_3$  to absorb visible light, which it could not do on its own. Figure 7(b) shows the UV-Vis transmission spectra for  $\text{TiO}_2\text{-NiO@In}_2\text{O}_3$  NCTFs with various molar ratios. The intensity of transmittance spectra in  $\text{In}_2\text{O}_3$  thin films increases with increasing wavelength, with increasing molar ratio of NiO because NiO is a good conductor of electricity. This means that the NiO-doped  $\text{In}_2\text{O}_3$  films have a lower resistivity than the pure  $\text{In}_2\text{O}_3$  films, and with decreasing molar ratio of  $\text{TiO}_2$  because  $\text{TiO}_2$  is a good absorber of light. This means that the  $\text{TiO}_2$ -doped  $\text{In}_2\text{O}_3$  films have a higher absorption coefficient than the pure  $\text{In}_2\text{O}_3$  films. A region of high transmittance; that comprises the visible range, so a wide range of wavelength ranging from 320 to 800 nm and is in the order of 90% for all  $\text{TiO}_2\text{-NiO@In}_2\text{O}_3$  NCTFs samples. As you can see, NiO has the largest bandgap and  $\text{TiO}_2$  has the smallest bandgap. This is why  $\text{In}_2\text{O}_3$  films with a higher

NiO content will transmit lighter than  $\text{In}_2\text{O}_3$  films with a higher  $\text{TiO}_2$  content. This high transparency is one of the essential characteristics and that fully justify the interest in  $\text{TiO}_2$  thin films [26]. The high transmittance of  $\text{TiO}_2$  thin films in the visible range is one of the essential characteristics making them so useful in various applications. Figure 7(c) illustrates the  $(ah)^2$  vs. photon energy (eV) plots for obtaining the band gap energy values. The band gaps shown in Figure 7 (c) and Table 2 of  $\text{TiO}_2\text{@In}_2\text{O}_3$  NCTFs with various molar ratio were changed from 4.079 for  $\text{TiO}_2\text{-NiO@In}_2\text{O}_3$  NCTFs (20:60:20) to 2.906 for  $\text{TiO}_2\text{-NiO@In}_2\text{O}_3$  NCTFs (60:20:20). Evidently, there was a gradual decrease in the  $\text{In}_2\text{O}_3$  band gap energy with  $\text{TiO}_2$  and NiO-loading. The decrease in the band gap energy of  $\text{In}_2\text{O}_3$  with  $\text{TiO}_2$  and NiO-loading has been used to improve the performance of  $\text{In}_2\text{O}_3$ -based photocatalysts for various applications, including  $\text{CO}_2$  reduction, water splitting, and organic pollutant degradation. The band gap energy of  $\text{In}_2\text{O}_3$  is 3.7 eV, which is higher than the band gap energy of  $\text{TiO}_2$  (3.2 eV). The band gap energy of the  $\text{In}_2\text{O}_3$  decreases when  $\text{In}_2\text{O}_3$  is loaded with  $\text{TiO}_2$ . This is because the  $\text{TiO}_2$  donates electrons to the  $\text{In}_2\text{O}_3$ , which narrows the band gap. The addition of  $\text{TiO}_2$  and NiO to the  $\text{In}_2\text{O}_3$  systems further decreases the band gap energy [27]. This is because NiO is a metal that has very low band gap energy (2.2 eV). The optical properties of  $\text{In}_2\text{O}_3$  are affected by the addition of  $\text{TiO}_2$  and NiO impurities. The  $\text{In}_2\text{O}_3$  transmittance increases as the NiO ratio increases and the  $\text{TiO}_2$  ratio decreases. This is because NiO has a larger bandgap than  $\text{TiO}_2$ , which means that it absorbs less light in the visible spectrum. As a result,  $\text{In}_2\text{O}_3$  films with a higher NiO content will transmit lighter.  $\text{TiO}_2$ , on the other hand, has a smaller bandgap than  $\text{In}_2\text{O}_3$ , which means that it absorbs more light in the visible spectrum. As a result,  $\text{In}_2\text{O}_3$  films with a higher  $\text{TiO}_2$  content will transmit less light.



**Figure 7:** (a) UV-Visible absorption spectra, (b) Transmittance spectra, and (c) Optical band gap energies of the prepared mixed TiO<sub>2</sub>-NiO@In<sub>2</sub>O<sub>3</sub> NCTFs for different molar ratio

**Table 2:** Elemental determination and optical band gap parameters of TiO<sub>2</sub>-NiO@In<sub>2</sub>O<sub>3</sub> NCTFs molar ratio: 50:30:20, 40:40:40, 30:50:20, 20:60:20, and 60:20:20, respectively

TiO <sub>2</sub> -NiO@In <sub>2</sub> O <sub>3</sub> NCTFs	Elements	Atomic %	Weight %	Optical band gaps
60:20:20	O	89.9	87.1	4.079
	Ti	7.5	2	
	Ni	1.3	4.8	
	In	1.3	6.1	
50:30:20	O	70.3	31.7	3.931
	Ti	6.2	3.2	
	Ni	16.9	41.7	
	In	6.6	23.4	
40:40:20	O	74.2	83.9	3.721
	Ti	5.6	1.5	
	Ni	18.3	4	
	In	1.9	10.6	
30:50:20	O	69.2	46.6	3.486
	Ti	4.2	0.3	
	Ni	22.1	34.4	
	In	4.5	18.8	
20:60:20	O	72.9	65.8	2.906
	Ti	3.1	2.1	
	Ni	22.6	24.4	
	In	1.4	7.7	

#### Photoluminescence analysis of TiO<sub>2</sub>-NiO@In<sub>2</sub>O<sub>3</sub> NCTFs on a glass substrate

Photoluminescence (PL) analysis is a useful technique for studying the optical properties of TiO<sub>2</sub>-NiO@In<sub>2</sub>O<sub>3</sub> NCTFs on a glass substrate. The PL spectra of the prepared pure and mixed TiO<sub>2</sub>-NiO@In<sub>2</sub>O<sub>3</sub> NCTFs for different molar ratios, obtained with excitation wavelength of 300 nm, 320 nm, and 350 nm, are illustrated in Figure 8 (a-c). The mixed TiO<sub>2</sub>-NiO@In<sub>2</sub>O<sub>3</sub> NCTFs (30:50:20) enhances the PL intensity emission compared to the other composition thin film

systems at 300 nm and 350 nm. This is because the specific composition of this system creates a favourable energy level alignment between the TiO<sub>2</sub>, NiO, and In<sub>2</sub>O<sub>3</sub> structures [28]. This alignment leads to a more efficient energy transfer from the excited TiO<sub>2</sub> nanoparticles to the NiO and In<sub>2</sub>O<sub>3</sub> nanoparticles, which results in a higher PL emission intensity [29]. As a result, the mixed TiO<sub>2</sub>-NiO@In<sub>2</sub>O<sub>3</sub> NCTFs (30:50:20) are a promising material for applications that require high PL emission intensity, such as light emitting diodes (LEDs) and solar cells.

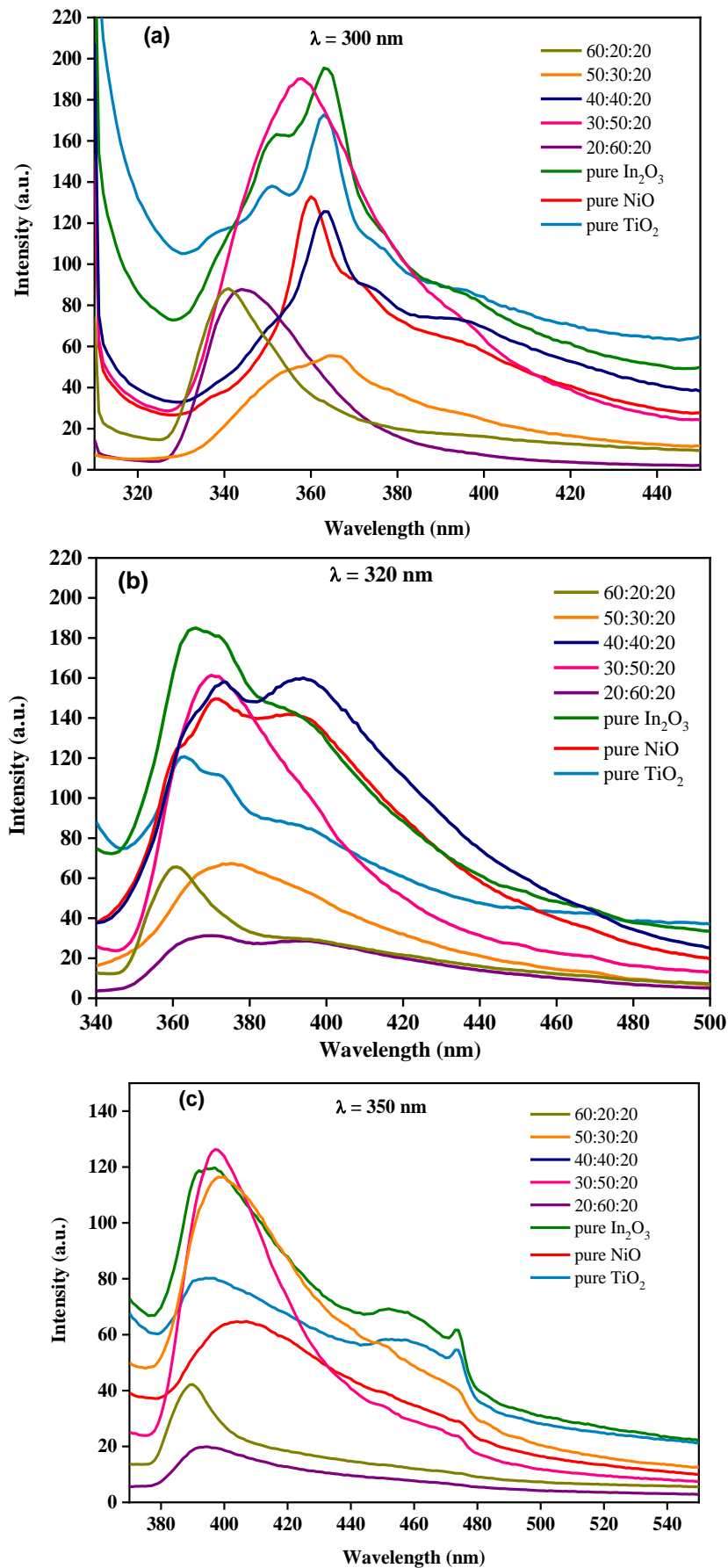


**Figure 8:** PL spectra of the prepared pure and mixed TiO<sub>2</sub>-NiO@In<sub>2</sub>O<sub>3</sub> NCTFs with different molar ratio for excitation wavelength of (a) 300 nm, (b) 320 nm, and (c) 350 nm

## Conclusion

To sum up, the TiO<sub>2</sub>-NiO@In<sub>2</sub>O<sub>3</sub> NCTFs synthesized via a cost-effective spray pyrolysis method demonstrate excellent gas sensing properties. By varying the composition of the materials, the thin films can be tailored to exhibit different characteristics. The SEM and EDX analysis verified the presence of nano-sized particles and a nanostructured surface in the films. Among the different compositions tested, the TiO<sub>2</sub>-NiO@In<sub>2</sub>O<sub>3</sub> NCTFs with ration (40:40:20) yielded the highest sensitivity, rapid response, and recovery times when detecting H<sub>2</sub>S gas. The sensor's resistance was measured under a bias voltage of 3V, and a significant decrease in resistance was observed upon the injection of H<sub>2</sub>S gas into the testing chamber, eventually reaching a new steady state, while NO<sub>2</sub> gas has opposite behavior. Overall, the study highlights the potential of these TiO<sub>2</sub>-NiO@In<sub>2</sub>O<sub>3</sub> NCTFs as efficient gas sensors with higher sensitive and selective applications. Optical properties of In<sub>2</sub>O<sub>3</sub> were affected by the TiO<sub>2</sub> and NiO addition. In fact, the transmittance increased as NiO ratio increased while TiO<sub>2</sub> ratio decreased.

## Disclosure Statement

No potential conflict of interest was reported by the authors.

## Funding

This study did not receive any specific grant from funding agencies in the public, commercial, or not-for-profit sectors.

## Authors' contributions

All authors contributed toward data analysis, drafting, and revising the paper and agreed to responsible for all the aspects of this work.

## Conflict of interest

The authors declare that they have no conflicts of interest in this article.

## ORCID

F. T Ibrahim

<https://orcid.org/0000-0001-9796-9990>

## References

- [1]. Azpiroz R., Carretero E., Cueva A., González A., Iglesias M., Pérez-Torrente J.J., In-flow photocatalytic oxidation of NO on glasses coated with nanocolumnar porous TiO<sub>2</sub> thin films prepared by reactive sputtering, *Applied Surface Science*, 2022, **606**:154968 [Crossref], [Google Scholar], [Publisher]
- [2]. A) Kaur M., Jain N., Sharma K., Bhattacharya S., Roy M., Tyagi A., Gupta S., Yakhmi J., Room-temperature H<sub>2</sub>S gas sensing at ppb level by single crystal In<sub>2</sub>O<sub>3</sub> whiskers, *Sensors and Actuators B: Chemical*, 2008, **133**:456 [Crossref], [Google Scholar], [Publisher] B) Mohajer F., Mohammadi Ziarani G., Badieli A., New advances on modulating nanomagnetic cores as the MRI-monitored drug release in cancer, *Journal of Applied Organometallic Chemistry*, 2021, **1**:143 [Crossref], [Google Scholar], [Publisher] C) Vaeli N., Laboratory experiment of the extraction of active pharmaceutical ingredients of *Oliveria decumbens* plant by supercritical method using the ultrasound process, *Eurasian Journal of Science and Technology*, 2021, **1**:242 [Crossref], [Publisher]
- [3]. Abegunde S. M., Idowu K. S., Enhanced Adsorption of Methylene Blue Dye from Water by Alkali-Treated Activated Carbon, *Eurasian Journal of Science and Technology*, 2023, **3**:109 [Crossref], [Publisher]
- [4]. A) Rajeh S., Souissi R., Ihzaz N., Mhamdi A., Bouguila N., Labidi A., Amlouk M., Guerhazi S., Physical investigations on Ni doping ZnO thin films along with ethanol response, *Journal of Materials Science: Materials in Electronics*, 2022, **33**:17513 [Crossref], [Google Scholar], [Publisher] B) Zamani Esfahlani M., charsouei S., A Review on the Process of Neuromotor Rehabilitation of Patients with Brain and spine Lesions and Developing Skills in Healthy People by Plasticity Analysis: systematic Review, *International Journal of Advanced Biological and Biomedical Research*, 2023, **11**:94 [Crossref],

- [Publisher] C) Roshanfekar H., A simple specific dopamine aptasensor based on partially reduced graphene oxide–Au NPs composite, *Progress in Chemical and Biochemical Research*, 2023, **6**:61 [Crossref], [Google Scholar], [Publisher]
- [5]. Li Z., Yao Z., Haidry A.A., Plecenik T., Xie L., Sun L., Fatima Q., Resistive-type hydrogen gas sensor based on TiO<sub>2</sub>: A review, *International journal of hydrogen energy*, 2018, **43**:21114 [Crossref], [Google Scholar], [Publisher]
- [6]. Feng W., Yang X., He Z., Liu M., Hydrogen sulfide gas sensor based on TiO<sub>2</sub>–ZnO composite sensing membrane-coated no-core fiber, *Journal of Physics D: Applied Physics*, 2021, **54**:135105 [Crossref], [Google Scholar], [Publisher]
- [7]. Katti V., Debnath A., Muthe K., Kaur M., Dua A., Gadkari S., Gupta S., Sahni V., Mechanism of drifts in H<sub>2</sub>S sensing properties of SnO<sub>2</sub>: CuO composite thin film sensors prepared by thermal evaporation, *Sensors and Actuators B: Chemical*, 2003, **96**:245 [Crossref], [Google Scholar], [Publisher]
- [8]. Ionescu R., Hoel A., Granqvist C., Llobet E., Heszler P., Low-level detection of ethanol and H<sub>2</sub>S with temperature-modulated WO<sub>3</sub> nanoparticle gas sensors, *Sensors and Actuators B: Chemical*, 2005, **104**:132 [Crossref], [Google Scholar], [Publisher]
- [9]. Ibupoto Z.H., Abbasi M.A., Liu X., AlSalhi M., Willander M., The synthesis of NiO/TiO<sub>2</sub> heterostructures and their valence band offset determination, *Journal of Nanomaterials*, 2014, **2014**:24 [Crossref], [Google Scholar], [Publisher]
- [10]. Saruhan B., Lontio Fomekong R., Nahirniak S., Influences of semiconductor metal oxide properties on gas sensing characteristics, *Frontiers in Sensors*, 2021, **2**:657931 [Crossref], [Google Scholar], [Publisher]
- [11]. Kampitakis V., Gagaoudakis E., Zappa D., Comini E., Aperathitis E., Kostopoulos A., Kiriakidis G., Binas V., Highly sensitive and selective NO<sub>2</sub> chemical sensors based on Al doped NiO thin films, *Materials Science in Semiconductor Processing*, 2020, **115**:105149 [Crossref], [Google Scholar], [Publisher]
- [12]. Chaudhari G., Bambole D., Bodade A., Padole P., Characterization of nanosized TiO<sub>2</sub> based H<sub>2</sub>S gas sensor, *Journal of materials science*, 2006, **41**:4860 [Crossref], [Google Scholar], [Publisher]
- [13]. Eranna G., Joshi B., Runthala D., Gupta R., Oxide materials for development of integrated gas sensors—a comprehensive review, *Critical Reviews in Solid State and Materials Sciences*, 2004, **29**:111 [Crossref], [Google Scholar], [Publisher]
- [14]. Petrov V.V., Ivanishcheva A.P., Volkova M.G., Storozhenko V.Y., Gulyaeva I.A., Pankov I.V., Volochaev V.A., Khubezhov S.A., Bayan E.M., High Gas Sensitivity to Nitrogen Dioxide of Nanocomposite ZnO–SnO<sub>2</sub> Films Activated by a Surface Electric Field, *Nanomaterials*, 2022, **12**:2025 [Crossref], [Google Scholar], [Publisher]
- [15]. Azpiroz R., Carretero, E., Cueva, A., González, A., Iglesias, M., Pérez-Torrente, J.J., In-flow photocatalytic oxidation of NO on glasses coated with nanocolumnar porous TiO<sub>2</sub> thin films prepared by reactive sputtering, *Applied Surface Science*, 2022, **606**:154968 [Crossref], [Google Scholar], [Publisher]
- [16]. Milani Fard M., Milani Fard A. M., Evaluation of Psychosocial Factors in the Coping Strategies of Patients with Inflammation, *Eurasian Journal of Science and Technology*, 2022, **2**:94 [Crossref], [Publisher]
- [17]. Leineweber A., Jacobs H., Hull S., Ordering of nitrogen in nickel nitride Ni<sub>3</sub>N determined by neutron diffraction, *Inorganic chemistry*, 2001, **40**:5818 [Crossref], [Google Scholar], [Publisher]
- [18]. Haunsbhavi K., Kumar K.D.A., Mele P., Aldossary O.M., Ubaidullah M., Mahesh H., Murahari P., Angadi B., Pseudo n-type behaviour of nickel oxide thin film at room temperature towards ammonia sensing, *Ceramics International*, 2021, **47**:13693 [Crossref], [Google Scholar], [Publisher]
- [19]. Zheng Z.Q., Zhu L.F., Wang B., In<sub>2</sub>O<sub>3</sub> nanotower hydrogen gas sensors based on both schottky junction and thermoelectronic emission, *Nanoscale research letters*, 2015, **10**:1 [Crossref], [Google Scholar], [Publisher]
- [20]. Malekkiani M., Heshmati Jannat Magham A., Ravari F., Dadmehr M., Facile fabrication of ternary MWCNTs/ZnO/Chitosan nanocomposite for enhanced photocatalytic degradation of methylene blue and antibacterial activity,

- Scientific Reports*, 2022, **12**:5927 [[Crossref](#)], [[Google Scholar](#)], [[Publisher](#)]
- [21]. Nasiri S., Rabiei M., Palevicius A., Janusas G., Vilkauskas A., Nutalapati V., Monshi A., Modified Scherrer equation to calculate crystal size by XRD with high accuracy, examples Fe<sub>2</sub>O<sub>3</sub>, TiO<sub>2</sub> and V<sub>2</sub>O<sub>5</sub>, *Nano Trends*, 2023, **3**:100015 [[Crossref](#)], [[Google Scholar](#)], [[Publisher](#)]
- [22]. Nurpeissova A., Choi M.H., Kim J.S., Myung S.T., Kim S.S., Sun Y.K., Effect of titanium addition as nickel oxide formation inhibitor in nickel-rich cathode material for lithium-ion batteries, *Journal of Power Sources*, 2015, **299**:425 [[Crossref](#)], [[Google Scholar](#)], [[Publisher](#)]
- [23]. Shankar P., Rayappan J.B.B., Gas sensing mechanism of metal oxides: The role of ambient atmosphere, type of semiconductor and gases-A review, *Science Letters Journal*, 2015, **4**:126 [[Google Scholar](#)], [[Publisher](#)]
- [24]. Salunkhe R., Shinde V., Lokhande C., Liquefied petroleum gas (LPG) sensing properties of nanocrystalline CdO thin films prepared by chemical route: effect of molarities of precursor solution, *Sensors and Actuators B: Chemical*, 2008, **133**:296 [[Crossref](#)], [[Google Scholar](#)], [[Publisher](#)]
- [25]. Ansari Z., Ko T.G., Oh J.H., CO-sensing properties of In<sub>2</sub>O<sub>3</sub>-doped SnO<sub>2</sub> thick-film sensors: effect of doping concentration and grain size, *IEEE Sensors Journal*, 2005, **5**:817 [[Crossref](#)], [[Google Scholar](#)], [[Publisher](#)]
- [26]. Tahir M., Tahir B., Amin N.A.S., Muhammad A., Photocatalytic CO<sub>2</sub> methanation over NiO/In<sub>2</sub>O<sub>3</sub> promoted TiO<sub>2</sub> nanocatalysts using H<sub>2</sub>O and/or H<sub>2</sub> reductants, *Energy Conversion and Management*, 2016, **119**:368 [[Crossref](#)], [[Google Scholar](#)], [[Publisher](#)]
- [27]. Essalhi Z., Hartiti B., Lfakir A., Siadat M., Thevenin P., Optical properties of TiO<sub>2</sub> Thin films prepared by Sol Gel method, *Journal of Materials and Environmental Science*, 2016, **7**:1328 [[Google Scholar](#)]
- [28]. Tahir M., Amin N.S., Performance analysis of nanostructured NiO-In<sub>2</sub>O<sub>3</sub>/TiO<sub>2</sub> catalyst for CO<sub>2</sub> photoreduction with H<sub>2</sub> in a monolith photoreactor, *Chemical Engineering Journal*, 2016, **285**:635 [[Crossref](#)], [[Google Scholar](#)], [[Publisher](#)]
- [29]. Uddin M.T., Nicolas Y., Olivier C., Jaegermann W., Rockstroh N., Junge H., Toupance, T., Band alignment investigations of heterostructure NiO/TiO<sub>2</sub> nanomaterials used as efficient heterojunction earth-abundant metal oxide photocatalysts for hydrogen production, *Physical Chemistry Chemical Physics*, 2017, **19**:19279 [[Crossref](#)], [[Google Scholar](#)], [[Publisher](#)]
- [30]. Yao N., Huang J., Fu K., Deng X., Ding M., Zhang S., Xu X., Li L., Reduced interfacial recombination in dye-sensitized solar cells assisted with NiO: Eu<sup>3+</sup>, Tb<sup>3+</sup> coated TiO<sub>2</sub> film, *Scientific Reports*, 2016, **6**:31123 [[Crossref](#)], [[Google Scholar](#)], [[Publisher](#)]

#### HOW TO CITE THIS ARTICLE

M. Abd Shahoodh, F.T. Ibrahim\*, S. Guermazi, Investigations on TiO<sub>2</sub>-NiO@In<sub>2</sub>O<sub>3</sub> Nanocomposite Thin Films (NCTFs) for Gas Sensing: Synthesis, Physical Characterization, and Detection of NO<sub>2</sub> and H<sub>2</sub>S Gas Sensors. *Chem. Methodol.*, 2023, 7(12) 994-1010.

DOI: <https://doi.org/10.48309/chemm.2023.428217.1741>

URL: [https://www.chemmethod.com/article\\_185111.html](https://www.chemmethod.com/article_185111.html)